Available online at www.sciencedirect.com
SCIENCE DIRECT®
Thermochimica Acta 432 (2005) 202–211
thermochimica acta
www.elsevier.com/locate/tca

Principles of quartz crystal microbalance/heat conduction calorimetry: Measurement of the sorption enthalpy of hydrogen in palladium

Allan L. Smith [a,b,*], Hamid. M. Shirazi [a]

[a] *Chemistry Department, Drexel University, Philadelphia, PA 19104, USA*
[b] *Masscal Corporation, 96 A. Leonard Way, Chatham, MA 02633, USA*

Received 19 February 2005; received in revised form 24 March 2005; accepted 30 March 2005
Available online 10 May 2005

Abstract

A sensitive new measurement technology is described which combines calorimetry, gravimetry, and rheology applied to chemical reactions in thin films: quartz crystal microbalance/heat conduction calorimetry (QCM/HCC). The quartz crystal microbalance/heat conduction calorimeters constructed so far simultaneously measure heat generation, mass uptake or release, and viscoelastic property changes in the same, sub-milligram solid film sample when gases interact with the film in an isothermal surrounding. It is possible to measure the energetics of formation of a single layer of adsorbed molecules on a gold surface with this technique. The principles of operation of both the mass and the heat flow sensor are described, and one implementation of the combined sensor and apparatus and its electronics is presented. Methods for calibration and the preparation of thin sample films are summarized. As an illustrative example, the determination of the sorption enthalpy of hydrogen in a 25 °C palladium film of 140 nm thickness is discussed in detail. Other examples of the operation of the QCM/HCC are tabulated.

Keywords: Quartz crystal microbalance; Heat conduction calorimetry; Sorption enthalpy; Palladium; Hydrogen

1. Introduction

The world is full of surfaces, and chemistry creates coatings on these surfaces in natural and man-made ways. Surface chemistry has been developed to give thin films at surfaces desirable properties—coatings and finishes, for example. Nature sometimes creates undesirable thin films, such as the biofilm called plaque. Many important chemical and biological processes occur in these films either in their production or use. For a solid film exposed to a gas, the gas may adsorb or dissolve in the film, or react catalytically at the surface. In a coating containing volatile components, the components evaporate by absorbing heat, the film mass decreases, and the viscous film becomes a glassy solid. Bacteria will grow as biofilms [1] on any surface accessible to nutrients.

In all these processes, heat is generated or absorbed, the thin film gains or loses mass, the viscoelastic properties of the solid film change, and the properties desired may be enhanced or destroyed. Quartz crystal microbalance/heat conduction calorimetry (QCM/HCC) was developed to study these chemical and biological processes in thin films [2–4].

The individual components of measurement in QCM/HCC each have long histories. In the early 19th century, accurate gravimetric measurements launched the quantitative interpretation of chemical processes in terms of atoms and molecules. Heat conduction calorimetry has been extensively used to measure adsorption energetics in solids. Gas sorption instruments or thermal gravimetric analysis can measure mass release in solids. Rheological measurements of shear and loss modulus are usually done at low frequency on large samples with dynamic mechanical analysis instrumentation. The quartz microbalance/calorimeter simultaneously measures heat generation, mass uptake or release, and viscoelastic property changes in the same,

* Corresponding author. Tel.: +1 5082418628; fax: +1 5083480303.
E-mail address: asmith@masscal.com (A.L. Smith).

0040-6031/$ – see front matter © 2005 Elsevier B.V. All rights reserved.
doi:10.1016/j.tca.2005.03.017

sub-milligram solid film sample when gases interact with the film in an isothermal surrounding.

2. The quartz crystal microbalance

A flat quartz disc with electrodes on both surfaces can be forced to oscillate in a transverse acoustic mode (motion parallel to the surface) by an RF voltage applied at the acoustical resonance frequency of the plate. This device is called a transverse shear mode (TSM) quartz plate resonator. The frequency of the fundamental mode is inversely proportional to plate thickness. For a plate thickness of 332 μm cut from a single crystal at a specified set of angles designated as the AT cut, the resonant frequency is 5.00 MHz in the transverse shear mode.

The development and applications of quartz plate resonators is a venerable field in electrical engineering, dating back to World War II. Quartz plate resonators are the basis of accurate measurements of time and are found in many commercial products from quartz timepieces to ultrastable frequency counters. TSM quartz plate resonators have been used as sensitive microbalances for thin adherent films since the late 1950's, following the pioneering work of Sauerbrey [5]. A TSM resonator whose frequency is continuously monitored when sample is deposited on its surface is known as a quartz crystal microbalance (QCM). The resonant frequency of a quartz TSM resonator of thickness h_q is:

$$f_0 = \frac{(\mu_q/\rho_q)^{1/2}}{2h_q} \tag{1}$$

where μ_q and ρ_q are the shear modulus and density of quartz. The shift in frequency due to deposition of a film of the same acoustic impedance as quartz is proportional to the deposited mass per unit area of the film, $\Delta m/A$:

$$\Delta f = -\frac{2f_0^2}{(\mu_q\rho_q)^{1/2}}\frac{\Delta m}{A} = -\frac{2f_0^2}{(\mu_q\rho_q)^{1/2}}h_f\rho_f = -Ch_f\rho_f. \tag{2}$$

For an AT-cut 5 MHz crystal at room temperature, $C = 56.6\ \text{Hz}/(\mu\text{g/cm}^2)$. QCMs have been used as film thickness monitors in vacuum deposition of metals and inorganic solids since the 1970s [6]. QCMs are useful because of their sub-nanogram sensitivity.

The electrical characteristics of an uncoated quartz QCM are well represented by a simple RLC damped resonator equivalent circuit with a complex impedance $\boldsymbol{Z_q}$. Using an impedance analyzer, it is possible to measure both the real and imaginary parts of $\boldsymbol{Z_q}$ for TSM resonators [7]. The width of the resonance for an uncoated 5 MHz resonator is 10–20 Hz, and the mechanical damping within the quartz that gives rise to this broadening can be determined by measuring the motional resistance R of the resonator, typically ∼10 Ω. When thin, stiff films are deposited on the QCM surface the increase in R is small, but softer, thicker films (i.e., rubbery polymers 5–10 μm thick) can increase R by hundreds or even thousands of ohms.

Since the mid 1980s [8] it has been recognized that TSM resonators can also operate in fluid media if electronic oscillator drivers of suitable gain are employed to excite the resonator and to offset the losses due to damping of the resonator by the fluid. When immersed in water, the motional resistance of a 5 MHz TSM resonator increases to ∼360 Ω. The electroacoustic theory of damped TSM resonators has been well developed by a number of groups [7,9–12]. For an infinite viscoelastic liquid in contact with the TSM [8], the frequency shift is

$$\Delta f_{liq} = -(2\rho_q h_q)^{-1}(\rho_l\eta_l f_0/\pi)^{1/2} \tag{3}$$

where ρ_l and η_l are the density and viscosity of the liquid. For a 5-MHz QCM immersed in water at 25 °C, $\Delta f_{liq} = -710$ Hz.

The impedance of a TSM resonator damped by a finite viscoelastic film can be described as the sum of two complex impedances:

$$\boldsymbol{Z} = \boldsymbol{Z}_q + \boldsymbol{Z}_L \tag{4}$$

where the acoustic load impedance due to the film $\boldsymbol{Z_L}$ contains both an inductive and a resistive part. Equations have been given [9–11] relating the complex impedance of a TSM resonator damped by a finite viscoelastic film to four parameters characterizing the film: the thickness h_f, the density ρ_f, the shear storage modulus G_f' and the shear loss modulus G_f''. Shear moduli are functions of the frequency at which they are measured, so for TSM resonators G' and G'' are determined at the QCM resonant frequency f_0. The determination of shear storage and loss moduli of thin viscoelastic films with TSM resonators has been reviewed [13,14]. Even though the basic physics of damped TSM resonators is well understood, the effort to determine G_f' and G_f'' from measurements of frequency shift and motional resistance change has been fraught with problems. For very thin, rigid films, the frequency shift contains no information on either G_f' or G_f'' because the Sauerbrey limit (Eq. (2)) is reached. For thicker and/or lossier films the frequency shift and motional resistance depend on G_f' and G_f'' in a complex manner not obvious by examining the equations.

The acoustic load impedance $\boldsymbol{Z_L}$ of a film measured at frequency $\omega = 2\pi f$, is

$$\boldsymbol{Z_L} = i\omega h_f\rho_f \tan\boldsymbol{\varphi}/\boldsymbol{\varphi}, \tag{5}$$

where $\boldsymbol{\varphi}$ is the (complex) acoustical phase shift,

$$\boldsymbol{\varphi} = \omega h_f\sqrt{\rho_f/\boldsymbol{G}} \tag{6}$$

Here, the modulus $\boldsymbol{G_f} = G_f' + iG_f''$ is also complex.

Two convenient experimental measures of the film properties are

(a) the difference in resonant frequency $\Delta f = f$ (crystal + film) − f (crystal)
(b) the difference in motional resistance $\Delta R = R$ (crystal + film) − R (film).

For thin films (the gravimetric region) the frequency shift Δf is proportional to $\rho_f h_f$, the mass per unit area of the film (the Sauerbrey relation, Eq. (2)). It is possible to define an "ideal rigid mass layer" with small acoustic phase shifts [11], for which the acoustic load impedance is purely imaginary and the Sauerbrey limit is reached.

The relationship between $\mathbf{Z_L}$ and the measured quantities is [15]

$$\Delta f/f_0 = -\mathrm{Im}(\mathbf{Z_L})/\pi Z_{cq} \tag{7}$$

$$\Delta R/4\pi f_0 L_q = \mathrm{Re}(\mathbf{Z_L})/\pi Z_{cq}. \tag{8}$$

Here, f_0, Z_{cq}, and L_q are the resonant frequency, acoustic impedance, and motional inductance of the bare quartz crystal.

Both Δf and ΔR are zero in the limit of zero film thickness. Voinova et al. [9] present equations for both quantities in a power series expansion in the thickness h_f. We have obtained equivalent results from expanding $\mathbf{Z_L}$ in a power series in h_f and collecting real and imaginary parts. The result for Δf and ΔR, to third order in h_f, is:

$$\frac{\Delta f}{f_0} = \frac{\rho_f h_f}{\rho_q h_q}\left\{1 + \frac{h_f^2}{3}\frac{4\pi f_0^2 \rho_f G'}{G'^2 + G''^2}\right\} \tag{9}$$

$$\Delta R = \frac{2L_q}{3\pi Z_q}\omega^4 \rho_f^2 h_f^3 \frac{G''}{G'^2 + G''^2}. \tag{10}$$

In the theory of viscoelastic solids, the compliance can be used instead of the modulus to quantify storage and loss behavior. The shear storage compliance is defined as:

$$J' = \frac{G'}{G'^2 + G''^2} \tag{11}$$

and the shear loss compliance is defined as:

$$J'' = \frac{G''}{G'^2 + G''^2}. \tag{12}$$

Thus, the thin film limit equations can be rewritten as:

$$\frac{\Delta f}{f_0} = \frac{\rho_f h_f}{\rho_q h_q}\left\{1 + \frac{4h_f^2 \pi f_0^2 \rho_f J'}{3}\right\} \tag{13}$$

and

$$\Delta R = \frac{2L_q}{3\pi Z_q}\omega^4 \rho_f^2 h_f^3 J''. \tag{14}$$

Eq. (13) is useful in estimating the thickness of compliant films at which deviations from the Sauerbrey equation are noticeable. Eq. (14) is useful in interpreting motional resistance measurements of thin films. In the thin film limit, the motional resistance change is proportional to the square of the film density, the cube of the film thickness, and the loss compliance of the film. For a 5-MHz QCM, typical values for L_q and Z_q are 0.0402 H and 8.84×10^6 Pa s/m, respectively.

3. Heat conduction calorimetry

In heat conduction calorimetry [16] the instantaneous thermal power, $P = \mathrm{d}Q/\mathrm{d}t$, generated within a sample is measured by means of a heat flow sensor located between the sample and a heat sink. The time integration of the thermal power signal $Q = \int P(t)\mathrm{d}t$ gives the total heat associated with a chemical process or reaction.

The heat flow sensors used in our calorimeters are thermocouple plates (TCP) [17]. A TCP is made up of a large number of thermocouples made of p- and n-doped bismuth telluride, connected in series electrically to give high output voltages but in parallel thermally to give a high ratio of output voltage to temperature difference over the TCP. The Seebeck coefficient a (V/K) for a single thermocouple is defined by $\Delta U = a\Delta T$. For a TCP we may define a device Seebeck coefficient, $E = Na$ where N is the number of thermocouples in a TCP[1].

Two properties of a TCP determine its sensitivity: the device thermal conductance K (W/K) and the device Seebeck coefficient: the calibration coefficient, ε, of an ideal heat flow calorimeter using a TCP is

$$\varepsilon = K/E, \text{ (W/V)} \tag{15}$$

For a real calorimeter some heat will be lost through heat flow paths other than the TCP, so a measured calibration coefficient will be somewhat higher than the one calculated with Eq. (15) [17]. The inverse of the calibration coefficient is termed the sensitivity of the instrument S (V/W).

At steady state the output voltage $U(t)$ from the heat flow sensor is proportional to the thermal power:

$$P(t) = \varepsilon U(t). \tag{16}$$

Determination of ε is discussed below.

Eq. (16) is sufficient for measurements when the thermal power changes slowly with respect to the time constant of the calorimeter. If we are interested in the kinetics of rapidly changing processes, Eq. (16) must be generalized. The Tian equation is employed for this purpose:

$$P(t) = \varepsilon\left(U(t) + \tau\frac{\mathrm{d}U(t)}{\mathrm{d}t}\right). \tag{17}$$

Here τ, the time constant of the calorimeter, is given by:

$$\tau = C/K, \tag{18}$$

where C is the heat capacity of the sample and its container. Note that the heat capacity of the sample only influences the time constant; the calibration coefficient is not changed. This is in contrast to adiabatic calorimetry in which the measured total heat Q for a process is proportional to the total heat capacity of sample and container.

[1] A useful discussion of the physical properties and operating formulae for thermoelectric devices can be found at the following URL: http://www.melcor.com./formula.htm.

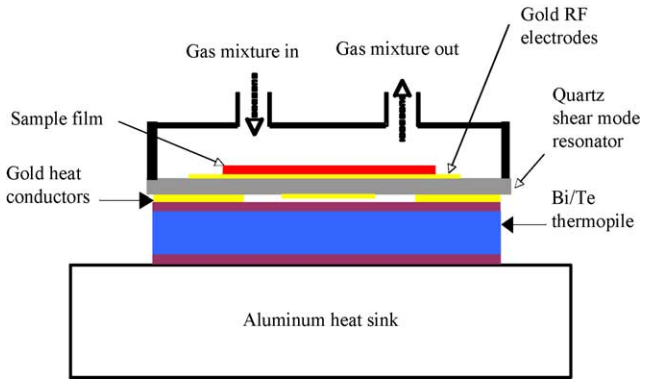

Fig. 1. Mass/heat flow sensor and sample chamber.

4. The mass/heat flow sensor

One realization of the mass/heat flow sensor that permits simultaneous measurements of mass change and heat flow from the same thin film sample is shown in Fig. 1. This is the sensor used in the Masscal^{TM} G1. To the ceramic plate constituting the top of the thermopile are applied thin layers of gold that separate the lower side of the shear mode resonator (QCM) from contact with a surface that would dampen its vibrations. They also function as electrodes to conduct RF power from the QCM oscillator electronics to the gold electrodes on the top and bottom of the QCM crystal, and as heat conduction paths from the QCM to the thermopile. Heat is also conducted through the air gap between the bottom of the QCM and the top of the thermopile. The thin film sample is applied to the top of the QCM crystal while outside the apparatus by a variety of techniques described below. A sample chamber (indicated only schematically here) rests on the outer edge of the QCM crystal through an o-ring seal, and contains ports for gas inlet and outlet. In the Masscal G1 the sample chamber volume is 0.30 mL. Typical gas flow rates of 10–20 cm^3/min allow for rapid change in sample gas composition within the chamber.

5. The apparatus

The mass/heat flow sensor and sample chamber must be thermally isolated from its surroundings in order to allow precise calorimetric measurements. Fig. 1 of ref. [18] and Fig. 1 of ref. [3] show schematic diagrams of the sample chamber of the Drexel quartz microbalance/calorimeter. In this instrument [2,19], the sample chamber/sensor combination is placed in a cylindrical brass enclosure and immersed in a constant temperature bath taken from a Tronac Model 1250 calorimeter (see Fig. 2 of ref. [3]). The bath regulates to ±0.0001 °C and may be varied from ambient temperature to 45 °C.

In the Masscal G1 [20], the sensor/sample chamber combination is mounted on an inner aluminum heat shield (mass 0.61 kg), which serves as the heat sink. This unit is encased in an outer aluminum shield (3.1 kg), which is surrounded by a 10-cm inch layer of high quality insulation. The total mass of the two shields is 3.67 kg. Heaters on two opposites sides of the outer shield are powered from a dc supply controlled by a high precision temperature controller capable of regulating the shield to better than ±0.005 °C from ambient to 110 °C. To maintain a 10 °C difference between ambient and the heat shield/calorimeter assembly requires 0.54 W of heater power. The thermal time constant for cooling the calorimeter and its heat shields is 17.3 h.

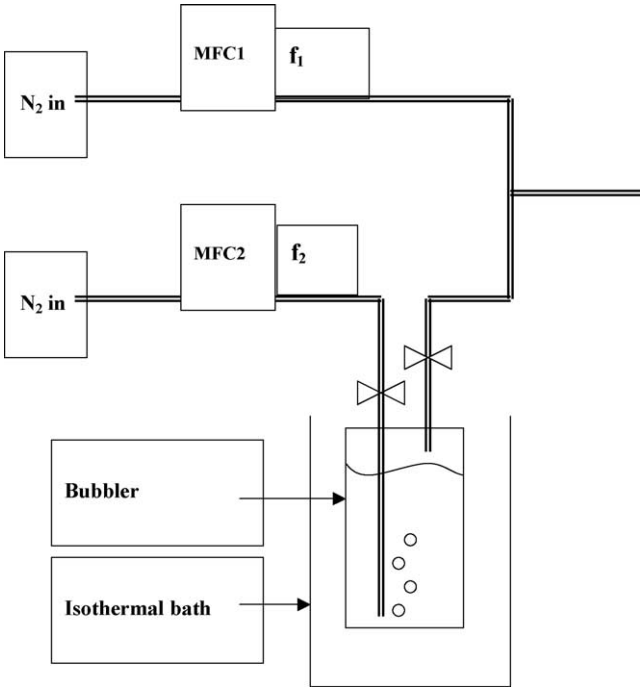

Fig. 2. Subsystem for introduction of gas mixture with a volatile component.

In QCM/HCC, changes in the measurement variables may be induced by spontaneous chemical or biological processes occurring within the sample film or by varying the gas composition in contact with the film in order to induce such processes. In both cases it is convenient to employ a software-based method of controlling gas composition. In both the Drexel instrument and the Masscal G1, this is accomplished with a separate subsystem based on mass flow controllers. Fig. 2 shows one realization of the subsystem, used to control water vapor activity. For a liquid whose vapor pressure at the temperature of the bubble-through container is P_{vap}, the partial pressure P_2 of the solvent in the output gas stream is [21]

$$P_2 = P_{vap}\left(\frac{f_2/(1-P_{vap})}{f_2/(1-P_{vap})+f_1}\right). \quad (19)$$

Here, f_1 and f_2 are the flow (in standard cm^3/min) of carrier gas through the two mass flow controllers, P_{vap} the vapor pressure of the liquid in the bubbler, and P_2 the partial pressure of the volatile component in the exit stream. The software for data acquisition and instrument control for both

the Drexel system and the Masscal system includes programs for variation of the partial pressure P_2 in both increasing and decreasing direction in stepwise or ramp fashion. This subsystem may also be used to produce two-component mixtures of non-condensible gases.

6. Electronics for data acquisition and control

Two firms provide RF oscillator electronics that can drive a 5-MHz quartz crystal into resonance and provide outputs of both the resonant frequency and the conductance voltage, an intermediate quantity from which motional resistance can be computed. These firms are Maxtek Inc. (Santa Fe Springs, CA) and Stanford Research Systems (Sunnyvale, CA). The Drexel University instrument employed Maxtek electronics (Model PLO-10 phase lock oscillator and Model RQCM research quartz crystal microbalance), and the Masscal G1 employs SRS electronics (the SRS QCM 100/25).

The thermopile output is measured with low-noise nanovolt amplifiers provided by EM Electronics (Brockenhurst, Hampshire, UK). For a 3-s integration time, typical achieved short-term rms noise levels are 0.2 μV, with drifts of <1 μV/h in well-equilibrated experiments.

Both the conductance voltage and the nanovolt amplifier output are digitized by 16-bit A/D converters on a National Instruments PCI multi-purpose data acquisition board. In the Drexel QCM/HCC, the frequency is measured with an HP 53131A frequency counter interface to a PC through an HPIB interface. In the Masscal G1, the frequency is determined by mixing with a stable oven-controlled oscillator and counting the frequency difference with the data acquisition board. A LabView program to acquire the data and control the experiment has been developed for both the Drexel instrument and the Masscal instrument; further details can be found in ref. [19] and in the Masscal G1 operations manual.

7. Calibration

7.1. Quartz crystal microbalance

For a film interacting with a gas, Eq. (13) provides a quantitative means of determining if any calibration is needed for the mass measurement. The numerator of the factor outside the brackets can be expressed as $m_{\text{film}}/A_{\text{film}}$, the mass per unit area of the film. If the second term inside the brackets is $\ll 1$, then the Sauerbrey equation is obeyed and the QCM is a true gravimetric device. The correction factor is proportional to the square of the film thickness, the film density and the film's shear compliance. Since most polymers are below their glass transition temperature at frequencies of 5 MHz, the time–temperature superposition principle [22,23] can be used to estimate the magnitude of J' and thus the thickness at which the Sauerbrey equation becomes inaccurate.

For QCMs interacting with liquid films, the problem is much more complex. Tsionsky et al. [12] discusses thoroughly the various limiting cases in which it is still possible to apply the Sauerbrey equation, but they are much more limited than in the case of film/gas interaction.

7.2. Thermopile

Although the dimensions and thermal properties of the material of which the thermpiles are made will determine its absolute sensitivity, the geometry of the thermopile, the QCM in close proximity with it, and the sample chamber sealing to the top of the QCM, will determine what fraction of the heat generated in the sample will flow down through the thermopile. It is thus important to determine experimentally the thermopile sensitivity $S = 1/\varepsilon$. In the Drexel University apparatus, the sensitivity was determined electrically by determining the QCM crystal's motional resistance and then exciting the crystal at resonance. Under these conditions, the thermal power dissipated by the quartz crystal is $V_{\text{rms}}^2/R_{\text{motional}}$, and a measurement of the mean square excitation voltage will determine the thermal power generated by the crystal. Since the crystal is driven to resonance in its normal operations, there will always be a contribution to the total thermal power signal from the heat generated within the crystal itself. This is calculable from R_{motional}, and it can often be 60–150 μW. If the motional resistance changes substantially in an experiment due to gas sorption, the this crystal thermal power component must be calculated and subtracted from the total signal to get the signal due to the gas/thin film interaction itself.

Because there are electronics challenges in determining precise values of the motional resistance for the purpose of thermopile calibration, we are developing an alternative method based on the dc power dissipation in a thin-film resistor on top of a quartz crystal [20].

8. Thin film sample preparation

In order for both mass and heat flow sensors to operate, the thin film sample must adhere to the top surface of the QCM and be of uniform thickness. Powder or polycrystalline samples cannot be used because such non-adherent materials do not follow the transverse motion of the QCM surface. The mechanical behavior of films on the quartz microbalance has been modeled by Kanazawa [24], who examined the amplitude of the shear displacement in the quartz crystal and in the overlying film for several cases. For a 1-V peak RF applied voltage typical of the Stanford Research Systems oscillator driver, the amplitude of the shear wave of a bare crystal is 132 nm, but this amplitude is reduced by a viscoelastic coating.

Several methods have been used to prepare thin film samples for the QCM: dip coating, drop coating, spray coating, spin coating, and self-assembled monolayer (SAM) formation. To achieve sample homogeneity and uniformity the best of these methods is spin-coating, if the film material is amenable to this treatment. The effect of non-uniform

thickness of films on the operation of the QCM has been treated by several authors [12,25].

Since the measured frequency difference $\Delta f = f$ (crystal + film) $- f$ (crystal) is proportional to the mass per unit area of the film, the total sample mass is obtained from Eq. (2) as $(\Delta m/A)A_{\text{film}}$ where A_{film} is the area of the film exposed to the gas.

9. Sorption of gases in solid thin films and at surfaces

Markova et al. [26] have presented applications of a double twin isothermal sorption calorimeter, which can be used to determine the sorption isotherm and the differential enthalpy of sorption for solid powders. The quartz microbalance/calorimeter described here can be used to determine both sorption enthalpies and sorption isotherms on the same thin film solid sample [18,27–29].

The sorption of a gas or volatile solvent A in a solid thin film or on a surface is represented by

$$A(g) \rightarrow A(\text{absorbed}) \tag{20}$$

Suppose that a thin film of mass m_{film} absorbs a mass δm of a gas of molar mass MM. The heat liberated by this process is:

$$\delta Q = \delta m \Delta H_{\text{sorption}}/\text{MM} \tag{21}$$

where $\Delta H_{\text{sorption}}$ is the differential enthalpy of sorption of the gas by the thin film. Since heat conduction calorimetry measures thermal power $P = \text{d}Q/\text{d}t$, we obtain:

$$P = \text{d}m/\text{d}t \Delta H_{\text{sorption}}/\text{MM}. \tag{22}$$

Thus, the thermal power is proportional to the time derivative of the mass signal, and the sorption enthalpy can be obtained from the proportionality constant.

An example of the relationship between the thermal power and mass signals is the absorption of hydrogen gas in a thin palladium film [19].

10. Hydrogen sorption in palladium

10.1. Introduction

The palladium/hydrogen system has been studied extensively as early as the 1860s. Palladium has a peculiar position among the group VIII metals. It has the highest hydrogen solubility and can absorb and desorb hydrogen under mild conditions very rapidly, forming a nonstoichiometric hydride, PdH_n [30]. Two different phases of the hydride can form at room temperature depending on the hydrogen composition: the α phase for low H/Pd atomic ratios (H/Pd < 0.015) and the β phase at higher hydrogen concentration (H/Pd > 0.7). The plateau region or miscibility gap of the sorption isotherm is a region in which a solid solution of both α and β phase exists (0.015 < H/Pd < 0.7 at 298 K). The critical point of the α/β phase diagram is $T_c = 563$ K and $P_c = 19$ bar [30].

Historically hydrogen sorption isotherms for palladium have been determined by one of three methods [30]. The pressure–composition–temperature (p–c–T) relationship has been studied from direct measurements of the partial pressure of hydrogen above a palladium sample as a known volume of the hydrogen gas is admitted into the sample container. Hydrogen can also be introduced into palladium by electrolysis. The cell potential of an electrochemical cell has been used to determine the hydrogen content of a palladium electrode. The current through two electrochemical cells separated by a palladium bielectrode membrane has been used to determine the diffusion coefficient of hydrogen in palladium. The hydrogen content can also be determined by measuring the electrical resistance of the palladium hydride.

The enthalpy of hydrogen sorption in palladium has been measured either directly by calorimetric methods or indirectly from p–c–T relationships (through the Clausius Clapeyron equation) and electrochemical experiments. Since hydrogen tends to absorb at very low pressures, distinguishing between the energetics of the α phase formation and the adsorption of hydrogen on the surface is not straightforward. Most of the measurements performed before the 1970s were in the α−β phase region. With improvements of the ultrahigh vacuum technology, the data for the α phase have increased over the past decades. Flanagan et al. [31] have determined the differential enthalpy for hydride formation,

$$\frac{1}{2}\text{H}_2(g) + \frac{1}{b-a}\text{PdH}_a \rightarrow \frac{1}{b-a}\text{PdH}_b \tag{23}$$

at 298 K to be -19.1 ± 0.5 kJ/mol H over the composition frange 0 < H/Pd < 0.7, in excellent agreement with more recent results [32].

10.2. Experimental

A thin palladium film was electrodeposited on the gold electrodes of a QCM. The shift in the oscillation frequency (9589 Hz) before and after the electroplating was used to determine the mass (221 μg) of the palladium film. The film thickness (141 nm) was calculated from the density of palladium (12.0 g/cc) and the film area (1.27 cm^2).

During the sorption experiments a N_2/H_2 gas mixture whose hydrogen composition was changed periodically using mass flow controllers under software control was passed over the Pd-coated QCM mounted in the sample chamber of the Drexel University apparatus. The H_2 used was of purity 99.9%. The result of one 14-h experiment is shown in Fig. 3, and the sixth and seventh cycles of this run are shown in more detail in Fig. 4. The sorption cycle consisted of 6 sorption/desorption steps, each of duration 550 s.

The mass and thermal responses of a clean gold surface on another reference QCM were measured for the same flow pattern used for Fig. 3. Resulting thermal power changes for each step change in hydrogen partial pressure were <0.3 μW and mass changes were <3 nm.

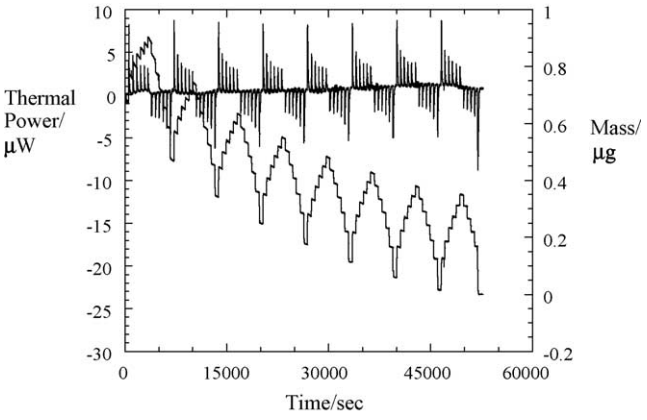

Fig. 3. Thermal power and mass change generated in a 140 nm palladium film subjected to cycles of increasing and decreasing partial pressures of H_2 in an N_2 carrier gas at 25 °C. Total pressure, 1.0 atm, initial H/Pd content unknown (see text).

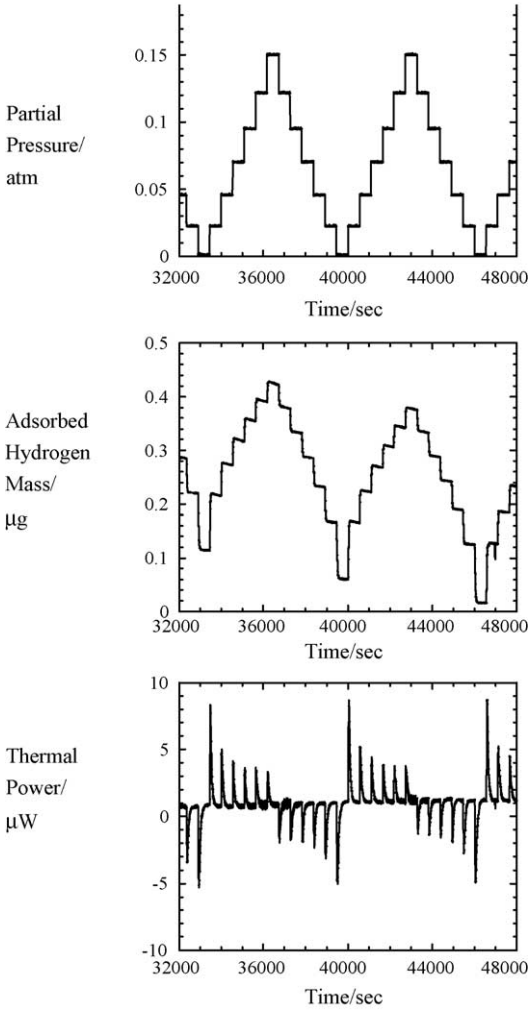

Fig. 4. Cycles 7 and 8 of Fig. 3—partial pressure of H_2, adsorbed hydrogen mass, and thermal power generated by H_2 sorption by a palladium film.

10.2.1. Discussion of results

In Figs. 3 and 4, the thermal power signal is indeed the time derivative of the mass signal, as predicted for sorption processes by Eq. (22). Diffusion of atomic hydrogen in palladium is far too fast to affect the observed kinetics. Diffusion coefficients for hydrogen in palladium for the α phase [33] are $1.3–3.1 \times 10^{-7}$ cm^2/s, and for a film 140 nm thick the time for equilibration of the hydrogen concentration is less than 1 μs.

There is a slow downward drift in the mass trace in Fig. 3, of −0.023% of the film mass per hour. This effect has been observed by other researchers and is attributed not to a mass loss but to the slow release of elastic stresses in the palladium film [34]. It is known that palladium undergoes a volume expansion of 11% during hydrogen sorption and in electroplating [30]. The palladium film is firmly bound to the gold/quartz layer. The volume expansion in the electroplating process results in a large strain on the QCM surface, which in turn has a substantial effect on the oscillation frequency of the QCM [35,36]. After the QCM is removed from the plating solution the stress is slowly relieved.

When such a stressed film is further stressed by hydrogen sorption, the shift in the oscillation frequency has two components: a gravimetrical frequency shift following Sauerbrey's relation and a frequency shift due to the change in surface stress. The exact magnitude of the stress-related frequency shift can be determined from measurements with two quartz plate resonators cut from a single crystal at different angles. If an AT-cut and BT-cut resonator pair is used, the total frequency shift for each QCM is given in the equation below [35,36]

$$\frac{\Delta f^{\mathrm{AT}}}{f_0} = \frac{K^{\mathrm{AT}}\Delta S^{\mathrm{AT}}}{\tau_{\mathrm{q}}^{\mathrm{AT}}} - \frac{\Delta M^{\mathrm{AT}}}{\rho_{\mathrm{q}}\tau_{\mathrm{q}}^{\mathrm{AT}}} \tag{24}$$

$$\frac{\Delta f^{\mathrm{BT}}}{f_0} = \frac{K^{\mathrm{BT}}\Delta S^{\mathrm{BT}}}{\tau_{\mathrm{q}}^{\mathrm{BT}}} - \frac{\Delta M^{\mathrm{BT}}}{\rho_{\mathrm{q}}\tau_{\mathrm{q}}^{\mathrm{BT}}} \tag{25}$$

where f_0^{AT} and f_0^{BT} are the original resonant frequencies of the AT-cut and BT-cut QCMs, Δf is the shift in the resonant frequency, ΔM is change in the mass loading, ΔS is the change in the lateral stress, K is a stress-related proportionality constant, and ρ and τ are the mass density and the quartz plate thickness, respectively. The constants K^{AT} and K^{BT} have almost the same magnitude but the opposite sign, $K^{\mathrm{AT}} = 2.75 \times 10^{-12}$ cm^2/dyn and $K^{\mathrm{BT}} = -2.65 \times 10^{-12}$ cm^2/dyn.

For an AT-cut QCM the hydride formation induced stress results in a decrease in the oscillation frequency as does an added mass loading, whereas for a BT-cut QCM the oscillation frequency will increase. Cheek and O'Grady [37] have shown that the shift in the resonant frequency of an AT-cut QCM overestimates the mass by a factor of ∼2 ($\Delta f_{\mathrm{actual\ mass}} = -185$ Hz, $\Delta f^{\mathrm{AT}} = -351$ Hz), where the same H loading in a palladium film with a BT-cut QCM will result in no significant frequency shift ($\Delta f_{\mathrm{actual\ mass}} = -185$ Hz,

$\Delta f^{BT} = -20$ Hz) [38]. Using an electrochemical quartz crystal microbalance Liu et al. [39] calculated the mass of absorbed hydrogen from the electrochemical current and were able to account for the shift in the oscillation frequency of a 10-MHz AT-cut QCM due to surface stress. A frequency shift of −423 Hz was separated into the gravimetrical (−210 Hz for 181 ng of hydrogen) and the surface stress components (−213 Hz for a surface stress of 1071 MPa).

Table 1 gives H/Pd ratios and differential enthalpies of hydrogen sorption (hydride formation and decomposition) during the two sorption cycles shown in Fig. 4. The mass m_i is the observed mass at the beginning of a step, and $\Delta m = m_{i+1} - m_i$ is the mass change attributed to hydride formation or decomposition during that step. The integrated heat Q is equal to $\int P(t)\mathrm{d}t$, where P is the thermal power signal, integrated over the time of the step. Differential sorption enthalpies per mole of absorbed atomic hydrogen were calculated for the individual steps from the integrated heats and mass changes.

The differential sorption enthalpies are a factor of 2 lower than accepted experimental values. We believe that this discrepancy is due to the residual stress in the palladium film imparted during the electroplating process. Since the double resonator technique was not used in this work, we used the relationships results summarized above to estimate the actual hydrogen mass in the palladium film in the present work. For the 5-MHz AT-cut QCM we take the actual mass to be 0.50 of the mass calculated from the Sauerbrey equation; i.e., the contribution of stress to the observed frequency shift is equal to the contribution from change in mass. We have no way to check this assumption without further experimentation.

Table 1
Differential hydrogen sorption enthalpies in a 141 nm palladium film, uncorrected for stress in the palladium[a]

m_i (μg)	Δm (ng)	Q (μJ)	H/Pd[b]	$\Delta_{sorption}H$ (kJ/mol)
0.114	102	−641.3	0.10	−12.6
0.216	57	−342.3	0.19	−12.0
0.273	43	−264.8	0.24	−12.3
0.316	39	−204.6	0.28	−10.5
0.355	36	−202.6	0.31	−11.3
0.391	32	−187.7	0.34	−11.7
0.423	−45	181.4	0.37	8.1
0.378	−46	204.8	0.33	8.9
0.332	−47	222.2	0.29	9.5
0.285	−53	263.3	0.25	9.9
0.232	−66	344.9	0.20	10.5
0.166	−106	630.0	0.15	11.9
0.060	105	−650.6	0.05	−12.4
0.165	58	−335.7	0.14	−11.6
0.223	45	−257.7	0.20	−11.5
0.268	38	−213.0	0.23	−11.2
0.306	36	−207.4	0.27	−11.5
0.342	34	−189.2	0.30	−11.1
0.376	−44	176.7	0.33	8.0
0.332	−44	195.1	0.29	8.9
0.288	−46	215.6	0.25	9.4
0.242	−53	259.9	0.21	9.8
0.189	−64	335.0	0.17	10.5
0.125	−109	635.5	0.11	11.7
0.016			0.01	

[a] Run 99-06-09-2, ref. [19].
[b] Nominal H/Pd ratio, uncorrected for initial hydrogen content of the film; see text.

Table 2
Differential sorption enthalpies of hydrogen in palladium (corrected for film stress)

Average H/Pd ratio	Hydride formation or decomposition	Average $\Delta_{sorption}H$ (kJ/mol H)	$\Delta_{sorption}H$ corrected for film stress
0.08	Formation	−12.5	−25.0
0.17		−11.8	−23.6
0.22		−11.9	−23.8
0.26		−10.9	−21.8
0.29		−11.4	−22.8
0.32		−11.4	−22.8
0.35	Decomposition	8.0	16.0
0.31		8.9	17.8
0.27		9.4	18.8
0.23		9.9	19.8
0.18		10.5	21.0
0.13		11.8	23.6
Mean of enthalpy of hydride formation			−23.3 ± 1.1
Mean of enthalpy of hydride decomposition			19.5 ± 2.6
Mean of absolute magnitude of sorption enthalpy			21.4 ± 2.8

In Table 2, we have averaged the results of each step from the two runs shown in Fig. 4, then applied the correction for film stress. Given the experimental uncertainties, we cannot identify any trend with increasing H/Pd ratio for either the formation or the decomposition enthalpies. The mean value of the absolute magnitude of all differential enthalpies, 21.4 ± 2.8 kJ/mol H, is in satisfactory agreement with the previous results of Flanagan et al. [31](19.1 ± 0.1 kJ/mol H) and of Sakamoto et al. [32] (18.6 ± 0.3 kJ/mol H).

In order to compare our measured values of enthalpies of hydrogen sorption with the literature values, the hydrogen content of the palladium film before exposure to hydrogen gas has to be known. It is known that an electroplated palladium film can contain moderate amounts of hydrogen, which form a chemically stable hydride at room temperature [40–42]. This residual hydrogen is usually removed by heating the palladium sample to a temperature above its critical temperature ($T_c \approx 300\,^{\circ}$C) in vacuum. Without thermal treatment of our sample and in the absence of a vacuum system in the gas flow cell of the QCM/HCC, it was impossible to remove all of the absorbed hydrogen. Therefore, the exact hydrogen content of the palladium film was not known. We could only estimate the range of the region of H/Pd ratio on the sorption isotherm based on the hydrogen partial pressure during the sorption/desorption cycles. For this reason, the change in mass due to hydrogen sorption is presented as a nominal H/Pd mole ratio, uncorrected for the unknown initial hydrogen content of the film.

Variations in the energetics and hydrogen uptake capacity of palladium [30] have been attributed to several factors: the degree of surface cleanliness, the presence of impurities in

the palladium sample or hydrogen gas, sample pretreatment, annealing, crystallinity and the number of defects in its lattice structure, and the geometry of the palladium sample: size and surface-to-volume ratio. Annealing of the palladium sample increases the reproducibility of the measured quantities for hydrogen sorption experiments, but it also reduces the hydrogen uptake capacity of palladium, since a relatively large quantity of hydrogen can reside in the defects in the lattice structure. One of the largest sources of scatter in the experimental results of hydrogen sorption is variation of the surface to volume ratio of palladium samples used [33,42]. Three different types of sites exist where hydrogen sorption can take place: sites at the surface of palladium, sites within the lattice structure of bulk palladium and sites within defects in the lattice structure, and each site exhibits different energetics for hydrogen sorption.

Our purpose in these measurements was not to make a careful, definitive determination of enthalpies of hydride formation in palladium, given the enormous literature on the subject. It was to show that quartz crystal microbalance/heat conduction calorimetry is a useful technique for studying the thermodynamics of gas sorption in solid thin film. Because the gas sorption process may change the materials characteristics of the film, the ability to do both gravimetric and calorimetric measurements on same sub-milligram sample with this measurement technology is a significant advantage.

11. Other modes of operation

11.1. Gas sorption by thin films

The data presented above are for sorption of hydrogen in palladium. The QCM/HCC has been used to measure thermodynamic and kinetic properties associated with sorption for a number of other systems, and Table 3 summarizes these studies with their associated references.

Table 3
Some applications of quartz crystal microbalance/heat conduction calorimetry

Field	Application
Coatings	Water uptake and softening of pharmaceutical film coat materials [45]
Molecular solids	Solubility and solvent uptake in C_{60} fullerene films [45]
Polymers	Thermodynamic and rheological property changes (plasticization) of polymer films upon sorption of solvents; sorption enthalpies, partition coefficients, and changes in shear and loss modulus; diffusion coefficients of volatile components in polymers [18,19]
Proteins	Water sorption isotherms and hydration enthalpies of lysozyme [28]. Phase transitions due to change of hydration levels of phosphate buffers in myoglobin/buffer films [46]. Label-free detection of the binding of the anticoagulant drug warfarin to a thin film of human serum albumen [47]
Self-assembled monolayers	Energetics of formation of self-assembled monolayers [4,19]
Heterogeneous catalysis	Reaction rate and mass build-up on a platinum catalyst during the hydrogenation of ethylene [48]
Microbiology	Detection of the early stages of bacterial growth on a nutrient medium by monitoring simultaneously the mass change and the metabolic heat evolution [47]

11.2. Mass change and heat flow at the surface of heterogeneous catalysts

For a bimolecular reaction

$$A(\mathrm{g}) + B(\mathrm{g}) \rightarrow [\text{absorbed intermediates}] \rightarrow \text{products} \quad (26)$$

catalysed at a solid surface, there is no simple relationship between heat flow and mass change as in Eq. (22) for gas sorption. The thermal power P or rate of heat liberation at the catalytic surface is related to the heterogeneous reaction rate by,

$$P = \Delta H_{\mathrm{rxn}} \mathrm{d}\xi/\mathrm{d}t \quad (27)$$

where ΔH_{rxn} is the enthalpy for the bimolecular reaction and ξ is the extent of reaction. Determining the variation of P with the concentrations of reagents A and B can give the order of the reaction and its catalyst turnover frequency, or heterogeneous rate constant. But the mass change at the surface cannot be predicted from the reaction stoichiometry; it must be measured. Often in catalytic reactions of hydrocarbons there is a build-up of carbonaceous material at the surface, termed catalytic fouling; in this case, the surface mass increases with time. But in other cases the reactive species are adsorbed layers pre-existing on the catalyst, which are depleted by the reaction, producing a mass decrease. Because of the sub-monolayer sensitivity of the QCM, the QCM/HCC is well-suited to monitoring catalytic processes. Table 3 gives an example of such a study.

11.3. Growth of microorganisms

All living systems generate metabolic heat at various rates during their life cycle. Biological microcalorimetry has been extensively used to monitor growth in bacteria [43]. Bacteria often show a proclivity to grow at surfaces rather than in bulk solution, forming biofilms in the process [1]. The QCM/HCC has been utilized to monitor the growth of *Escherica coli* on a nutrient-containing agar surface applied as a thin film on the QCM (see Table 3). Changes in all three properties—mass, heat flow, and motional resistance—are a measure of the growth process.

11.4. Chemical reactions in surface films in contact with aqueous solutions

Reactions of soluble species with surface films are important in designing chemical [44] and biological [14] sensors as well as in studying bioadhesion, biopolymers, and lipid bilayers. QCM/HCC has been employed to measure ligand–protein and protein–protein interactions at surfaces and to characterize a widely used two-step zero-length crosslinking procedure involving esterification reactions at surfaces. Table 3 contains the details and references.

12. Conclusions

The challenges in converting this new measurement technology from a unique laboratory apparatus to an instrument useable in a chemistry or materials science lab have been overcome with the introduction of the Masscal^{TM}G1. Feedback and advice from early adopters of the technology will be crucial in determining whether quartz crystal microbalance/heat conduction calorimetry will become another useful tool for the surface scientist or thin film technologist.

Acknowledgements

The original concept for the mass/heat flow sensor was developed while ALS was on sabbatical leave at Lund University in 1997. Professor Ingemar Wadsö of Lund University designed the core of the first apparatus, which was developed further at Drexel by graduate students Hamid Shirazi, S. Rose Mulligan, and Jun Tian. Early support at Drexel University for the development of the QCM/HCC was received from Merck Corporation, from the DuPont Corporation, and from Sandia Corporation. The U.S. Department of Energy provided a Phase I SBIR Grant to Masscal Corporation in 2003 to further develop the technology.

References

[1] L. Hall-Stoodley, J.W. Costerton, P. Stoodley, Nat. Rev. Microbiol. 2 (2004) 95.
[2] A.L. Smith, H. Shirazi, I. Wadso, in: Recent Advances in the Chemistry and Physics of Fullerenes and Related Materials, vol. 98–8, Electrochem. Soc., San Diego, CA, 1998, p. 576.
[3] A.L. Smith, H.M. Shirazi, J. Thermal Anal. Calorimetry 59 (2000) 171.
[4] A.L. Smith, S.R. Mulligan, J. Tian, H. Shirazi, J.C. Riggs, IEEE Frequency Control Symposium, IEEE, Tampa, FL, 2003.
[5] G. Sauerbrey, Z. Physik 155 (1959) 206.
[6] C.-S. Lu, A.W. Czanderna, Applications of Piezoelectric Quartz Crystal Microbalances, Elsevier, New York, 1984.
[7] R. Lucklum, P. Hauptmann, Faraday Dis. 107 (1997) 123.
[8] K.K. Kanazawa, J.G. Gordon, Anal. Chem. 57 (1985) 1770.
[9] M.V. Voinova, M. Jonson, B. Kasemo, Biosens. Bioelectron. 17 (2002) 835.
[10] S.J. Martin, H.L. Bandey, R.W. Cernosek, A.R. Hillman, M.J. Brown, Anal. Chem. 72 (2000) 141.
[11] R. Lucklum, P. Hauptmann, R.W. Cernosek, IEEE International Frequency Control Symposium 2001 (2001) 542.
[12] V. Tsionsky, L. Daikhin, M. Urbakh, E. Gileadi, in: A.J. Bard, I. Rubenstein (Eds.), Electroanalytical Chemistry, vol. 22, Marcel Dekker, New York, Basel, 2003, p. 1.
[13] R. Lucklum, P. Hauptmann, IEEE International Frequency Control Symposium 2001 (2001) 408.
[14] A. Janshoff, H.-J. Galla, C. Steinem, Angew. Chem. Int. Ed. 39 (2000) 4004.
[15] R. Borngraeber, J. Schroeder, R. Lucklum, P. Hauptmann, IEEE Frequency Control Symposium 2001 (2001) 443.
[16] I. Wadsö, Chem. Soc. Rev. 1997 (1997) 79.
[17] P. Bäckman, M. Bastos, D. Hallén, P. Lönnbro, I. Wadsö, J. Biochem. Biophys. Methods 28 (1994) 85.
[18] A.L. Smith, S.R. Mulligan, H.M. Shirazi, J. Polym. Sci. Part B Polym. Phys. 42 (2004) 3893.
[19] H.M. Shirazi, Ph.D. thesis, Drexel University, Philadelphia, PA, 2000. p. 336.
[20] 2004.
[21] D. Berling, B. Jonsson, G. Olofsson, J. Sol. Chem. 28 (1999) 693.
[22] J.D. Ferry, Viscoelastic Properties of Polymers, Wiley, New York, 1980.
[23] J.D. Ferry, J. Polym. Sci., Part B Polym. Phys. 37 (1999) 620.
[24] K.K. Kanazawa, Faraday Soc. Dis. 107 (1997) 77.
[25] A.C. Hillier, D.A. Ward, Anal. Chem. 64 (1992) 2539.
[26] N. Markova, E. Sparr, L. Wadsö, Thermochim. Acta 374 (2001) 93.
[27] J. Tian, A.L. Smith, in: P.V. Kamat, D.M. Guldi, K.M. Kadish (Eds.), PV 2002-12 Fullerenes: The Exciting World of Nanocages and Nanotubes, vol. 12, Electrochemical Society, Philadelphia, 2002, p. 255.
[28] A.L. Smith, H.M. Shirazi, S.R. Mulligan, Protein Structure and Molecular Enzymology, Biochim. Biophys. Acta (BBA) 1594 (2002) 150.
[29] A.L. Smith, H.M. Shirazi, J. Thermal Anal. Calorimetry 59 (2000) 171.
[30] T.B. Flanagan, W.A. Oates, Ann. Rev. Mater. Sci. 21 (1991) 269.
[31] T.B. Flanagan, W. Luo, J.D. Clewley, J. Less-Common Metals 172 (1991) 42.
[32] Y. Sakamoto, M. Imoto, K. Takai, T. Yanaru, K. Ohshima, J. Phys.-Condens. Matter 8 (1996) 3229.
[33] V. Breger, E. Gileadi, Electrochim. Acta 16 (1971) 177.
[34] R.V. Bucur, M.V., T.B. Flanagan, Surf. Sci. 54 (1976) 477.
[35] E.P. EerNisse, J. Appl. Phys. 43 (1972) 1330.
[36] E.P. EerNisse, J. Appl. Phys. 44 (1973) 4482.
[37] G.T. Cheek, W.E. O'Grady, J. Electroanal. Chem. Interfacial Electrochem. 277 (1990) 341.
[38] G.T. Cheek, W.E. O'Grady, J. Electroanal. Chem. 368 (1994) 133.
[39] S.Y. Liu, Y.H. Kao, Y. Su, T.P. Perng, J. Alloys Comp. 293–295 (1999) 468.
[40] A. Czerwinski, R. Marassi, S. Zamponi, J. Electroanal. Chem. Interfacial Electrochem. 316 (1991) 211.
[41] C. Christofides, A. Mandelis, J. Appl. Phys. 66 (1989) 3986.
[42] M.W. Lee, R. Glosser, J. Appl. Phys. 57 (1985) 5236.
[43] J.P. Belaich, in: A.E. Beezer (Ed.), Biological Microcalorimetry, Academic Press, London, 1980, p. 1.
[44] A.J. Ricco, R.M. Crooks, G.C. Osbourn, Acc. Chem. Res. 31 (1998) 289.
[45] J. Tian, Ph.D. thesis, Drexel University, Philadelphia, 2003, 300 pp.
[46] S.R. Mulligan, Ph.D. thesis, Drexel University, Philadelphia, 2003, 400 pp.
[47] A.L. Smith, G. Zilberman, in: M. Rich (Ed.), 32nd Annual Conference of the North American Thermal Analysis Society, NATAS - CD-ROM, Williamsburg, VA, 2004.
[48] A.L. Smith, F.C. Smith, H.M. Shirazi, in: M.J. Rich (Ed.), 32nd Annual Conference of the North American Thermal Analysis Society, NATAS - CD-ROM, Williamsburg, VA, 2004.